International Journal of Engineering Trends and Technology
ISSN: 2231 – 5381 / https://doi.org/10.14445/22315381/IJETT-V71I2P236

Volume 71 Issue 2, 341-348, February 2023

Original Article

Bird Mating Optimizer with Deep Learning-based Tuberculosis Detection using Chest Radiographs

K. Manivannan[1], S. Sathiamoorthy[2]

[1]*Department of Computer and Information Science, Annamalai University, Annamalai Nagar.*
[2]*Annamalai University PG Extension Centre, Villupuram. Tamilnadu.*

[1]*Corresponding Author : manik81au@gmail.com*

Received: 12 November 2022 Revised: 08 February 2023 Accepted: 18 January 2023 Published: 25 February 2023

Abstract *- Tuberculosis (TB) is a prolonged lung illness that affects by pneumonia cases and results in a high mortality rate. TB detection is a tedious process that is primarily due to different kinds of manifestations, namely focal lesions, large opacities, aggregation, cavities, CXR image nodules, and small opacities. Early and accurate detection of TB is of considerable importance, or else it could be life-threatening. Machine learning (ML) is a subdivision of computing that analyses algorithms with the capability to "learn." The study of health interest images with deep learning (DL) could not be constrained to the usage of medical diagnosis. In this study, we propose a bird mating optimizer with deep learning-based TB detection and classification (BMODL-TBDC) system on chest radiographs. The presented BMODL-TBDC technique applies median filtering (MF) for noise removal. For feature extraction, the Xception architecture is used with the BMO algorithm as a hyperparameter optimizer. Finally, boosted convolutional autoencoder (BCAE) is applied for TB detection purposes. The simulation outcome of the BMODL-TBDC approach on the benchmark medical database reports promising performance over other recent systems with respect to various measures.*

Keywords *– Tuberculosis, Chest radiographs, Machine learning, Deep learning, Bird mating optimizer.*

1. Introduction

Tuberculosis (TB), otherwise termed consumption, is a chronic infectious disease arising from the germ named *Mycobacterium tuberculosis* [1]. The bacteria usually affect the lung region and other parts of the body. The air can spread TB and is curable and preventable when diagnosed at an initial stage; otherwise, it may result in death. Tests, namely chest X-ray (CXR) or process of a sputum sample, are done to identify TB disease patients [2]. A very exciting appraisal of the progression of processing techniques and medical image analysis can be found since the 1980s. Image classification is simply defined as the task of deriving classes of data from an image [3]. There were 2 forms of classification they are unsupervised and supervised. The supervised classification begins in a collection of recognized classes; such classes should be categorized as per the variables set by measuring them in individuals that membership of one class could not provide doubts [4], whereas the unsupervised categorization does not accomplish any class, though it becomes essential to decide the count of classes that has to be accomplished and let a statistical process describe them [5].

In medical practice, chest radiographs will be inspected by experts for diagnosing TB [6]. But this is a subjective and time-consuming process [7]. Subjective inconsistency in disease diagnosis from radiographs can be unavoidable. Significantly, CXR images of TB were often miscategorized to other illnesses of the same radiologic pattern that causes inaccurate treatment to the patients and thus worsens their health [8]. There exists a lack of skilled radiotherapists in the lower resource countries (LRCs), particularly in the non-urban zones. In this context, a CAD system serves a significant part of the mass screening of pulmonary TB by examining CXR images [21]. The availability of deep convolutional neural networks (CNN) and large-scale labelled data made great achievements in image recognition. CNN's highly representative allow data-driven, hierarchical image features that are studied from trained data; however, acquiring data in the medicinal image field as broadly annotated, as ImageNet will remain a challenge [9,10].

This study proposes a bird mating optimizer with deep learning-based TB detection and classification (BMODL-TBDC) technique on chest radiographs. The presented BMODL-TBDC technique applies median filtering (MF) for noise removal. For feature extraction, the Xception architecture is used with the BMO algorithm as a hyperparameter optimizer. Finally, boosted convolutional autoencoder (BCAE) is applied for TB detection purposes.

The experimental validation of the BMODL-TBDC technique occurs on a benchmark medical database.

2. Literature Review

Nguyen et al. [11] explored the efficacy of transfer learning (TL) on medicinal imaging for the detection of TB. The author shows an enhanced methodology for TL over the classical approach of utilizing ImageNet weight. Also, the author discovers that the lower-level feature from ImageNet weight is not beneficial for imaging tasks for modalities such as X-rays and presents a novel approach for obtaining lower-level features by training the model in multi-class multi-label scenarios. The authors in [12] developed an innovative TB recognition method that fuses handcrafted features with deep features (CNN) through Ensemble Learning. The handcrafted feature was extracted through Gabor Filter, and the deep feature was extracted through the pretrained DL model.
Chowdary [13] introduces an automated technique for the analysis of TB in posteroanterior CXR. This is a 2-phase methodology. Initially, the lung region is segmented in CXRs with the help of a graph cut model; next, the TL of VGG-16 fused with BiLSTM was utilized for extracting higher-level discriminatory features in the segmentation lung region, and later classifier can be done through FC layer. The authors in [14] applied CNN and DL to categorize the image of the TB culture test. As the database is smaller and imbalanced, a TL technique was implemented.

In addition, as the recall of non-negative classes is a vital metric for this application, the authors present a 2-stage classifier approach for boosting the outcomes.

Ravi et al. [22] examine a detailed search and investigation of 26 pre-trained CNN techniques utilizing a newly published and huge open dataset of TB Xray.[18] Several visualization approaches were implemented to depict optimal features learned with pretrained CNN approaches. The authors [16] introduce a CAD method exploiting a pre-training CNN as extracting feature and logistic regression (LR) technique for automatically analyzing the chest radiographs to offer an appropriate and correct analysis of several images. The chest radiographs can be pre-processed beforehand to extract distinct features and, afterwards, provide a classifier to identify that image can be infected.

3. The Proposed Model

In this study, we have introduced a novel BMODL-TBDC methodology for TB detection and classification on chest radiographs. The presented BMODL-TBDC technique utilized the MF approach for noise removal. For feature extraction, the Xception architecture is used with the BMO algorithm as a hyperparameter optimizer. Finally, the BCAE is applied for TB detection purposes. Fig. 1 illustrates the flow process of the BMODL-TBDC algorithm.

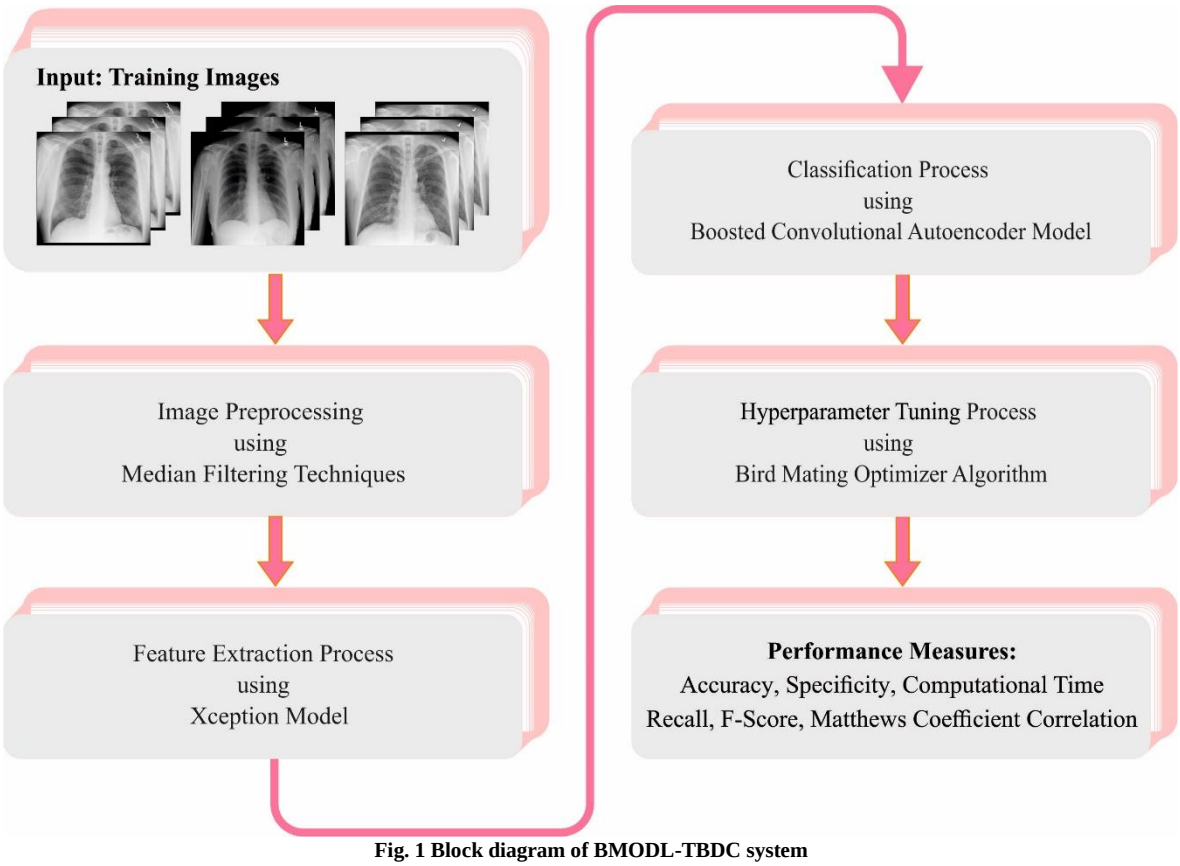

Fig. 1 Block diagram of BMODL-TBDC system

3.1. Feature Extraction Module

In this article, the Xception model was exploited for producing feature vectors. In the Xception framework, unlike the Inception framework, a convolutional process with depthwise separable convolution has been employed [17]. This kind of convolution layer has pointwise and depthwise convolution layers. At first, every filter individually processes a single channel of the input images; then, a filter size of 1x1 dimension iterates each input point. The Xception model uses depthwise separable convolution in different ways; in other words, 1x1 convolution is first utilized, and later channel-wise spatial convolution is used.

Xception framework comprises three architectures: Entry, middle, and exit flows. These three structure consists of fourteen models (2, 4, and 8 models, correspondingly) having overall 36 convolutional layers. There exist residual connections in the module except for the initial model of entry flow and the final model of exit flow. The Xception framework initiates with an entry flow that contains 4 modules, and every module has two convolutional layers. Initially, convolution is done by 64 and 32 filters with 3x3 dimensions. Next, the separable convolutional layer is realized with 128, 256, and 728 filters in 3x3 dimensions. Then accept the image size of 299x299x3 dimension as input in the entry flow and create a size of 19x19x728 feature maps at the output. Three separable convolutional modules with 728 filters in 3x3 dimensions are reiterated eight times in the middle flow. Middle flow constructs 19x19x728 feature maps at the output. The feature maps, the output of the middle flow, are provided as input to the exit flow. Exit flow contains two modules. Initially, the separable convolutional layer is done with 1024 and 728 filters in 3x3 dimensions; then, it can be done with 2048 and 1536 filters. Later, the framework is terminated with the addition of the FC layer.

The hyperparameter tuning of the Xception system occurs using the BMO algorithm. BMO is an approach inspired by the population algorithm. It is recommended to society for certain problems, and every society member is regarded as a possible solution and is termed a bird [23]. Generally, the gene of higher quality is possessed by females that are classified into different sets, such as polygyny, promiscuous, and monogamy. The female who poses genes of higher quality has further opportunities to be selected.

$$x_b = x + w^* r^* (x_j - x). \tag{1}$$

And if $r_1 > mcf$

$$x_b(c) = l(c) - r_2^* (l(c) - u(c)). \tag{2}$$

Where C denotes the random integer among 1 and n, the brood result represented as xb, the weighted of time-varying for defining the consequence of female can be denoted as $\mathcal{W}$, r is equivalent to the vector of $1 \times d$ where every component constructed randomly within zero and one influence the element of $(\chi_j - x)$, n characterizes the problem dimension. The factor of control mutation differs from zero to one and is specified as by^{mcf}, random number is specified as r_i that is within zero and one. Lastly, the upper bound of the component is denoted as u, whereas the lower one is denoted as l.

Polygyny type indicates mating amongst one male with more than one female. The key characteristic of extra-pair interaction is to attain better genes to brood as follows.

$$\chi_b = x + w^* \sum_{j=1}^{n_i} r_j^* (x_j - x). \tag{3}$$

Where n_i denotes the count of interested birds, χ_i characterizes the $j\text{-}th$ interesting bird. Note that the similar computation formula of monogamous is executed for the promiscuous type.

Every female raises the brood without the aid of males in the parthenogenesis type. Here, the female tries to pass-through through the preferred gene for her brood, and it can be expressed as follow:

$$\chi_b(i) = \chi(i) + \mu^* (r_2 - r_3)^* x(i). \tag{4}$$

Otherwise

$$\chi_b(i) = x(i). \tag{5}$$

Where μ denotes the size step and mcf_p specifies the controlling aspect for parthenogenetic mutation. In this study, the same computation formula of polygyny is executed for the polyandry type.

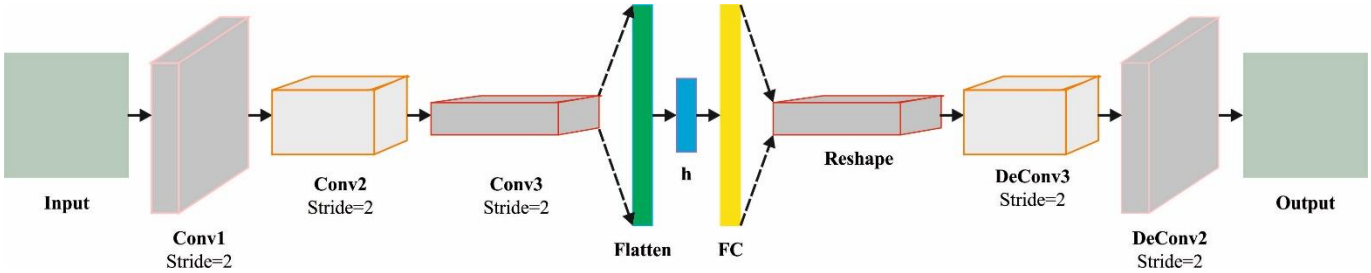

Fig. 2 Structure of CAE

3.2. TB Classification Module

The BCAE model is used in this study for the TB classification process. BCAE is an unsupervised feature learning model [19]. CAE is a multi-level feature extraction method focused on determining the inner data of the image. In comparison to dense AE, CAE exploits the spatial-locality of the original image and minimizes the probability of over-fitting caused by parameter redundancy. The presented CAE involves encoding and decoding blocks. The conversion from the original images to hidden layers is termed the encoding procedure. The decoding aims to mine the inner data compressed from the input dataset, extract it as a useful feature, and recreate the input dataset from the extracted feature. Fig. 2 illustrates the framework of CAE.

In this work, $X = \{x_1, x_2, \dots, x_n\} \in R^{H \times W \times D}$ applied as input tensor, whereas W, and H stand for depth, width, and height of inputs correspondingly, and n denotes the pixel number. X comprises image patches (x_i^*) with a dimensional of $7 \times 7 \times D (x_i^* \in R^{7 \times 7 \times D})$ that are extracted from the input images. Then, all the patches are fed into the encoding blocks. For input x_i^*, the hidden layer mapping (hidden depiction) of k^{th} feature maps are represented as follows:

$$h^k = \sigma(x_i^* * W^k + b^k) \tag{6}$$

In Eq. (6), b denotes the bias, σ represents the activation function (ReLU), and $*$ corresponds to the $2D$ convolutional layer:

$$y = \sigma\left(\sum_{k \epsilon H} h^k * \widetilde{W}^k + \tilde{b}^k\right) \tag{7}$$

Whereas $\tilde{b}$ characterizes the bias to all the input channels, and h represents the encoding feature map. $\overline{W}$ refers to the transposal of W, and y shows the prediction value. To evaluate the variable vector $\theta_{CAE} = \{W^k, \widetilde{W}^k, b^k, \tilde{b}^k\}$, the subsequent loss function must minimalize:

$$E(\theta) = \frac{1}{n}\sum_{i=1}^{n} \| x_i^* - y_i \|_2^2 \tag{8}$$

To minimalize the loss function, its gradient regarding the convolution window parameter $(W, \widetilde{W}\ b, \tilde{b})$ must be evaluated using the following expression:

$$\frac{\partial E(\theta)}{\partial W^k} = x^* * \delta h^k + h^k * \delta y \tag{9}$$

$$\frac{\partial E(\theta)}{\partial b^k} = \delta h^k + \delta y$$

Now, δh and δy represent the deltas of hidden state and reconstruction, correspondingly. Then, the weight is upgraded based on the adaptive learning rate method (ADAM). Lastly, the final parameter of CAE is assessed. The resultant feature map of the encoding blocks is considered a deep feature.

4. Results and Discussion

The simulation result of the BMODL-TBDC method can be tested by exploiting the TB Chest X-ray database [20], which holds 4200 samples and two classes, as defined in Table 1. Fig. 3 represents the sample images.

The classification results of the BMODL-TBDC technique are investigated with respect to the confusion matrix in Fig. 4. The figure represented that the BMODL-TBDC system has accurately recognized the presence of normal and TB images under all aspects.

Table 2 offers comprehensive TB classifier outcomes of the BMODL-TBDC algorithm on 80% and 20% of TRS/TSS.

Fig. 5 represents the TB classification outcome of the BMODL-TBDC system on 80% of TRS. In a normal class, the BMODL-TBDC model has gained $accu_{bal}$ of 99.39%, $sens_y$ of 99.39%, $spec_y$ of 96.74%, F_{score} of 99.38%, and MCC of 96.20%. Meanwhile, in the tuberculosis class, the BMODL-TBDC method has acquired $accu_{bal}$ of 96.74%, $sens_y$ of 96.74%, $spec_y$ of 99.39%, F_{score} of 96.83%, and MCC of 96.20%.

Table 1. Details on database

Class Name	No. of Samples
Normal	3500
TB	700
Sample count	**4200**

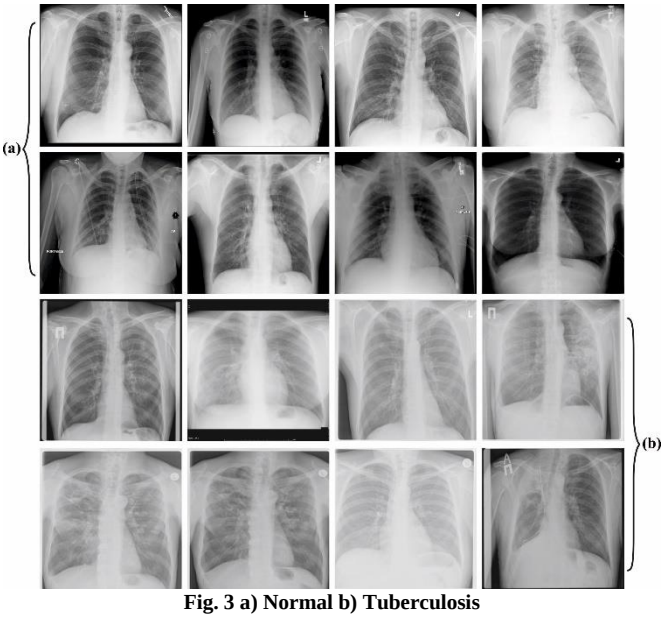

Fig. 3 a) Normal b) Tuberculosis

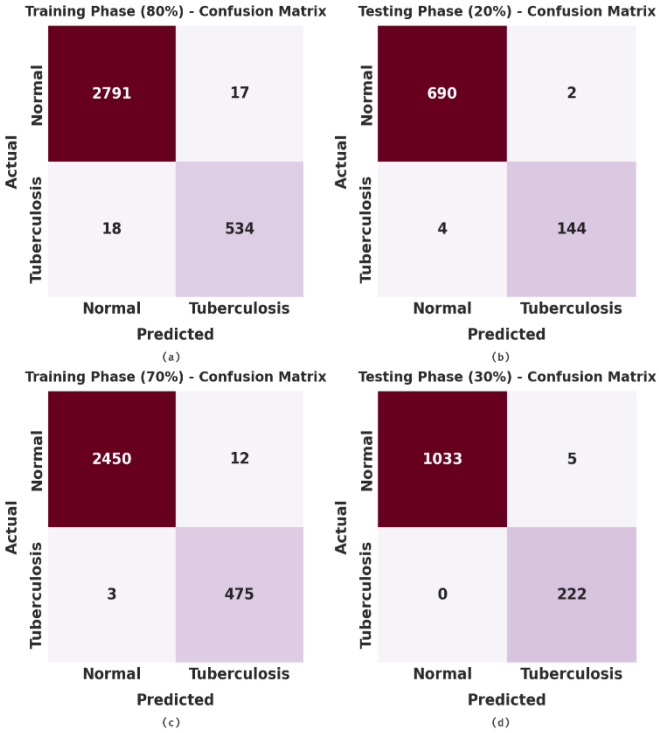

Fig. 4 Confusion matrices of BMODL-TBDC methodology (a-b) TRS/TSS of 80:20 and (c-d) TRS/TSS of 70:30

Table 2. TB classifier result of BMODL-TBDC algorithm under 80:20 of TRS/TSS

Class	$Accuracy_{bal}$	Sensitivity	Specificity	F-Score	MCC
Training Phase (80%)					
Normal	99.39	99.39	96.74	99.38	96.20
Tuberculosis	96.74	96.74	99.39	96.83	96.20
Average	**98.07**	**98.07**	**98.07**	**98.10**	**96.20**
Testing Phase (20%)					
Normal	99.71	99.71	97.30	99.57	97.53
Tuberculosis	97.30	97.30	99.71	97.96	97.53
Average	**98.50**	**98.50**	**98.50**	**98.76**	**97.53**

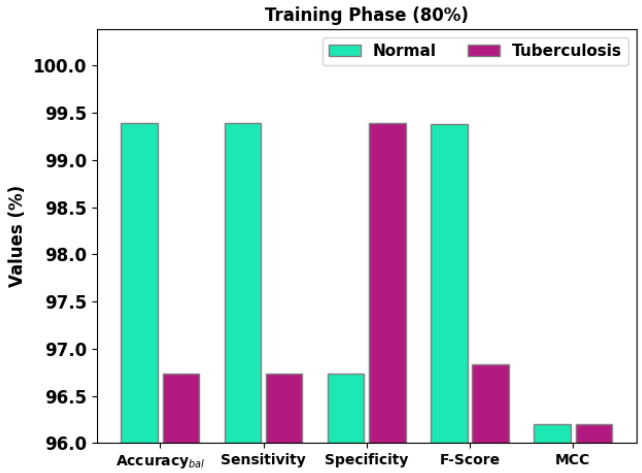

Fig. 5 TB classification result of BMODL-TBDC algorithm in 80% of TRS

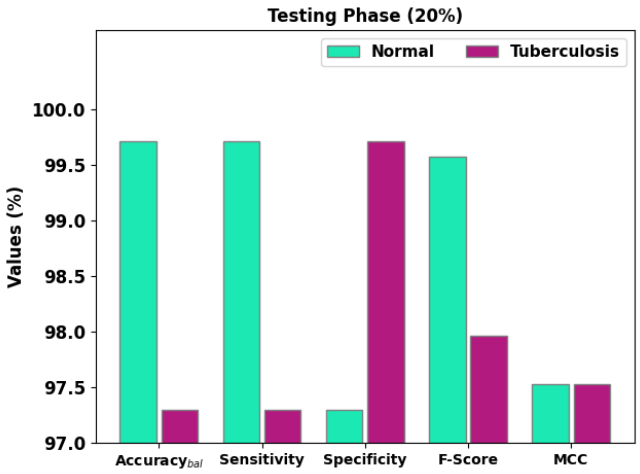

Fig. 6 TB classification result of BMODL-TBDC algorithm in 20% of TSS

Table 3. TB classifier outcome of BMODL-TBDC methodology on 70:30 of TRS/TSS

Class	$Accuracy_{bal}$	Sensitivity	Specificity	F-Score	MCC
Training Phase (70%)					
Normal	99.51	99.51	99.37	99.69	98.15
Tuberculosis	99.37	99.37	99.51	98.45	98.15
Average	**99.44**	**99.44**	**99.44**	**99.07**	**98.15**
Testing Phase (30%)					
Normal	99.52	99.52	100.00	99.76	98.65
Tuberculosis	100.00	100.00	99.52	98.89	98.65
Average	**99.76**	**99.76**	**99.76**	**99.32**	**98.65**

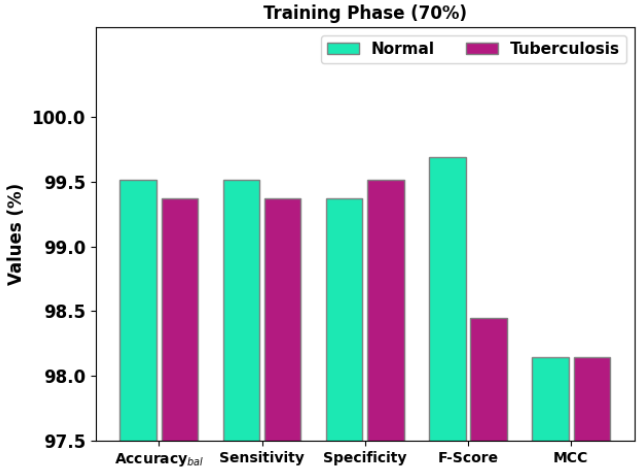

Fig. 7 TB classification result of BMODL-TBDC algorithm in 70% of TRS

Fig. 6 shows the TB classification outcome of the BMODL-TBDC methodology on 20% of TSS. In a normal class, the BMODL-TBDC approach has attained $accu_{bal}$ of 99.71%, $sens_y$ of 99.71%, $spec_y$ of 97.30%, F_{score} of 99.57%, and MCC of 97.53%. In the meantime, in tuberculosis class, the BMODL-TBDC approach has

acquired $accu_{bal}$ of 97.30%, $sens_y$ of 97.30%, $spec_y$ of 99.71%, F_{score} of 97.96%, and MCC of 97.53%.

Table 3 presents comprehensive TB classification outcomes of the BMODL-TBDC approach on 70% and 30% of TS datasets.

Fig. 7 implies the TB classification results of the BMODL-TBDC algorithm on 70% of TRS. In a normal class, the BMODL-TBDC technique has obtained $accu_{bal}$ of 99.51%, $sens_y$ of 99.51%, $spec_y$ of 99.37%, F_{score} of 99.69%, and MCC of 98.15%. In the meantime, in tuberculosis class, the BMODL-TBDC approach has acquired $accu_{bal}$ of 99.37%, $sens_y$ of 99.37%, $spec_y$ of 99.51%, F_{score} of 98.45%, and MCC of 98.15%.

Fig. 8 displays the TB classifier result of the BMODL-TBDC methodology on 30% of TSS. In a normal class, the BMODL-TBDC technique has obtained $accu_{bal}$ of 99.52%, $sens_y$ of 99.52%, $spec_y$ of 100%, F_{score} of 99.76%, and MCC of 98.65%. In parallel, on tuberculosis class, the BMODL-TBDC method has acquired $accu_{bal}$ of 100%, $sens_y$ of 100%, $spec_y$ of 99.52%, F_{score} of 98.89%, and MCC of 98.65%.

The TR_{acc} and VL_{acc} accomplished by the BMODL-TBDC algorithm in the test database is defined in Fig. 9. The figure values displayed by the BMODL-TBDC methodology have attained higher values of TR_{acc} and VL_{acc}. Predominantly the VL_{acc} is greater than TR_{acc}.

The TR_{loss} and VL_{loss} attained by the BMODL-TBDC methodology in the test database are depicted in Fig. 10. The experimental values denoted by the BMODL-TBDC methodology are established minimal values of TR_{loss} and VL_{loss}. Seemingly, the VL_{loss} is lesser than TR_{loss}.

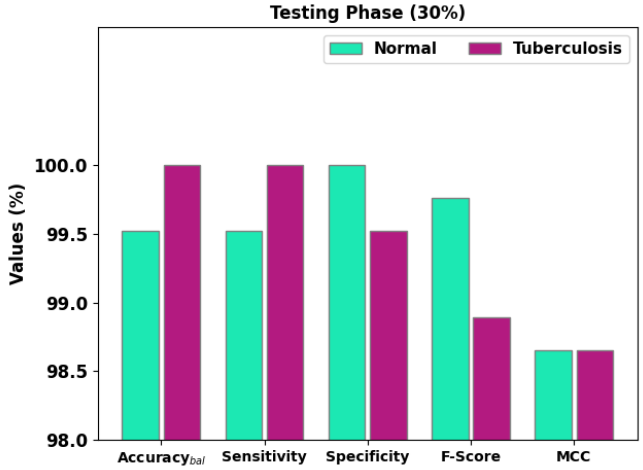

Fig. 8 TB classification result of BMODL-TBDC algorithm in 30% of TSS

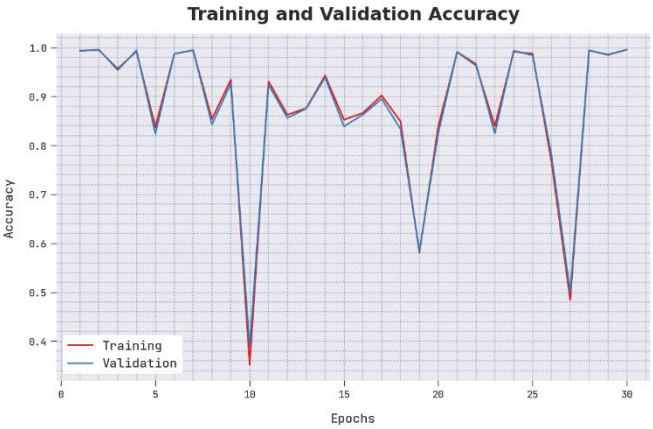

Fig. 9 TR_{acc} and VL_{acc} analysis of the BMODL-TBDC algorithm

Fig. 10 TR_{loss} and VL_{loss} analysis of the BMODL-TBDC algorithm

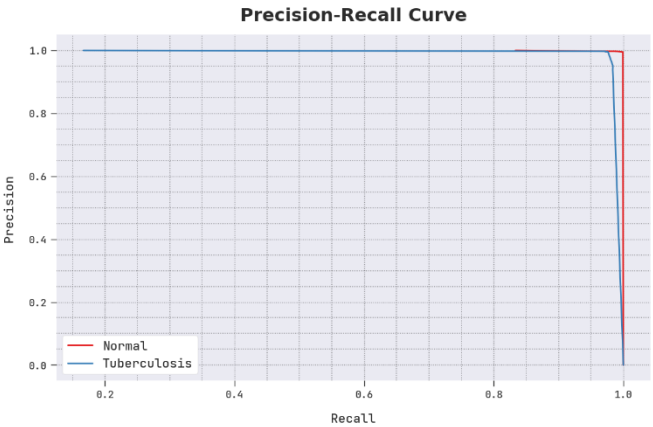

Fig. 11 PR outcome of BMODL-TBDC algorithm

An evident precision-recall (PR) inspection of the BMODL-TBDC system in the test database is given in Fig. 11. The figure exhibits that the BMODL-TBDC system has led to greater values of PR values in two class labels.

Table 4 and Fig. 12 demonstrate a comparative $accu_y$ examination of the BMODL-TBDC system.

Table 4. Accuracy analysis of BMODL-TBDC algorithm with recent systems

Methods	$Accu_y$
ResNet-l8	96.53
ResNet-50	97.63
ResNet-101	97.98
Inception-V3	98.91
Vgg-19	98.60
DenseNet-201	98.32
BMODL-TBDC	99.76

The result shows that the ResNet18 approach has reached lower $accu_y$ of 96.53%. Next, the ResNet50 and ResNet101 models have resulted in moderately closer $accu_y$ of 97.63% and 97.98% correspondingly. Although the Inceptionv3, VGG19, and DenseNet201 models have obtained reasonable $accu_y$ of 98.91%, 98.60%, 98.32%, and 99.76% correspondingly.

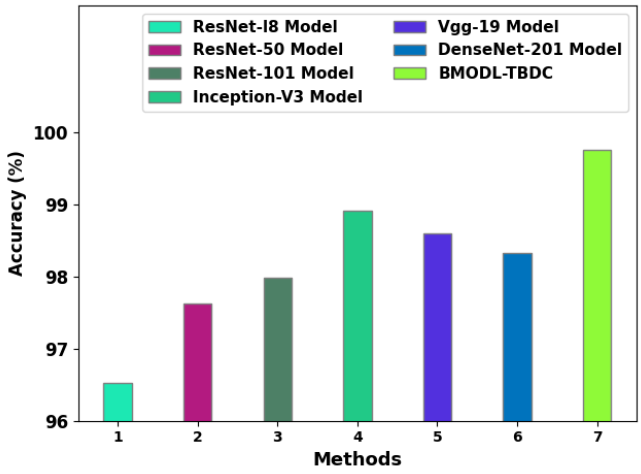

Fig. 12 Accuracy analysis of BMODL-TBDC algorithm with recent systems

Finally, a comparative computation time (CT) inspection of the BMODL-TBDC with recent techniques takes place in Table 5 and Fig. 13. The simulation outcomes signified that the BMODL-TBDC algorithm had reached a lower CT of 9.22s. In contrast, the other ResNet18, ResNet50, ResNet101, Inceptionv3, VGG19, and DenseNet-201 algorithms are depicted higher CT of 23.20s, 25.10s, 15.90s, 25s, 23.40s, and 20.30s correspondingly. Thus, the BMODL-TBDC algorithm has depicted maximal TB classifier results.

Table 5. CT analysis of BMODL - TBDC algorithm with recent systems

Methods	Computational Time (sec)
ResNetl8 Model	23.20
ResNet50 Model	25.10
ResNet101 Model	15.90
InceptionV3 Model	25.00
Vgg19 Model	23.40
DenseNet201 Model	20.30
BMODL-TBDC	09.22

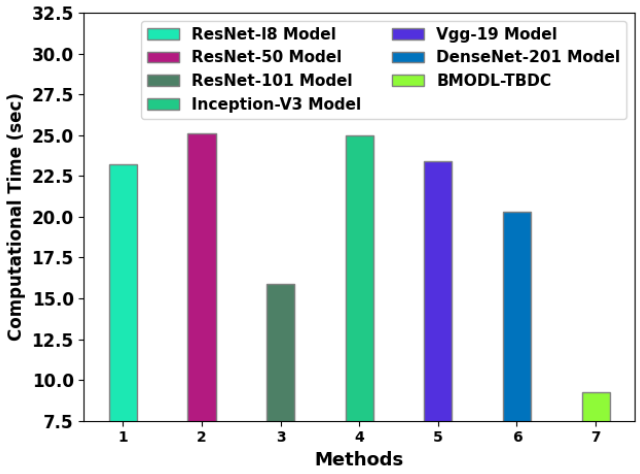

Fig. 13 CT analysis of BMODL-TBDC algorithm with recent systems

5. Conclusion

In this study, we have introduced a novel BMODL-TBDC technique for TB detection and classification on chest radiographs. The presented BMODL-TBDC technique utilized the MF approach for noise removal. For feature extraction, the Xception architecture is used with the BMO algorithm as a hyperparameter optimizer.

Finally, the BCAE is applied for TB detection purposes. The experimental validation of the BMODL-TBDC technique on a benchmark medical dataset reports promising performance over other state-of-the-art models in terms of different measures.

Thus, the presented BMODL-TBDC technique can be utilized for real-time TB diagnosis. In the future, advanced DL algorithms can be used to optimize the detection rate of the BMODL-TBDC technique.

References

[1] Mostofa Ahsan, Rahul Gomes, and Anne Denton, "Application of a Convolutional Neural Network Using Transfer Learning for Tuberculosis Detection," *2019 IEEE International Conference on Electro Information Technology (EIT), IEEE,* pp. 427-433, 2019. *Crossref*, http://doi.org/10.1109/EIT.2019.8833768

[2] Omar Faruk et al., "A Novel and Robust Approach to Detect Tuberculosis Using Transfer Learning," *Journal of Healthcare Engineering*, 2021. *Crossref*, https://doi.org/10.1155/2021/1002799

[3] Linh T. Duong et al., "Detection of Tuberculosis from Chest X-Ray Images: Boosting the Performance with Vision Transformer and Transfer Learning," *Expert Systems with Applications*, vol. 184, p.115519, 2021.

[4] Shuangquan Li et al., "Health Checkup could Reveal Chronic Disorders with Support from Artificial Intelligence," *International Journal of Engineering Trends and Technology*, vol. 67, no. 11, pp. 8-15, 2019. *Crossref*, https://doi.org/10.14445/22315381/IJETT-V67I11P202

[5] Dilmurod Nabiev, and Khayit Turaev, "Study of Synthesis and Pigment Characteristics of the Composition of Copper Phthalocyanine with Terephthalic Acid," *International Journal of Engineering Trends and Technology*, vol. 70, no. 8, pp. 1-9, 2022. *Crossref*, https://doi.org/10.14445/22315381/IJETT-V70I8P201

[6] Shwetambari Borade et al., "Deep Scattering Convolutional Network for Cosmetic Skin Classification," *International Journal of Engineering Trends and Technology*, vol. 70, no. 7, pp. 10-23, 2022. *Crossref*, https://doi.org/10.14445/22315381/IJETT-V70I7P202

[7] Khairul Munadi et al., "Image Enhancement for Tuberculosis Detection Using Deep Learning," *IEEE Access*, vol. 8, pp. 217897-217907, 2020. *Crossref*, https://doi.org/10.1109/ACCESS.2020.3041867

[8] Michail Mamalakis et al., "DenResCov-19: A Deep Transfer Learning Network for Robust Automatic Classification of COVID-19, Pneumonia, and Tuberculosis from X-Rays," *Computerized Medical Imaging and Graphics*, vol. 94, p.102008, 2021. *Crossref*, https://doi.org/10.1016/j.compmedimag.2021.102008

[9] ParveenChandna, Anju Dhiman, and Dalip Singh Dhiman, "HRCT Imaging of Pulmonary Tuberculosis," *SSRG International Journal of Medical Science*, vol. 9, no. 5, pp. 1-12, 2022. *Crossref*, https://doi.org/10.14445/23939117/IJMS-V9I5P101

[10] Thi Kieu Khanh Ho et al., "Utilizing Pretrained Deep Learning Models for Automated Pulmonary Tuberculosis Detection using Chest Radiography," *Asian Conference on Intelligent Information and Database Systems, Springer, Cham*, pp. 395-403, 2021. *Crossref*, https://doi.org/10.1007/978-3-030-14802-7_34

[11] Quang H. Nguyen et al., "Deep Learning Models for Tuberculosis Detection from Chest X-Ray Images," *2019 26th International Conference on Telecommunications (ICT), IEEE*, pp. 381-385, 2019. *Crossref*, https://doi.org/10.1109/ICT.2019.8798798

[12] Muhammad Ayaz, Furqan Shaukat, and Gulistan Raja, "Ensemble Learning based Automatic Detection of Tuberculosis in Chest X-Ray Images Using Hybrid Feature Descriptors," *Physical and Engineering Sciences in Medicine*, vol. 44, no. 1, pp. 183-194, 2021. *Crossref*, https://doi.org/10.1007/s13246-020-00966-0

[13] G Jignesh Chowdary et al., Class Dependency based Learning using Bi-LSTM Coupled with the Transfer Learning of VGG16 for the Diagnosis of Tuberculosis from Chest X-Rays," *arXiv preprint arXiv:2108.04329*, 2021. *Crossref*, https://doi.org/10.48550/arXiv.2108.04329

[14] Ray-I Chang, Yu-Hsuan Chiu, and Jeng-Wei Lin, "Two-Stage Classification of Tuberculosis Culture Diagnosis using Convolutional Neural Network with Transfer Learning," *The Journal of Supercomputing*, vol. 76, no. 11, pp. 8641-8656, 2020. *Crossref*, https://doi.org/10.1007/s11227-020-03152-x

[15] J. Anto Germin Sweeta, and Dr. B. Sivagami, "Contemporary Techniques in Digital Image Processing," *SSRG International Journal of Computer Science and Engineering*, vol. 6, no. 11, pp. 43-46, 2019. *Crossref*, https://doi.org/10.14445/23488387/IJCSE-V6I11P109

[16] Mustapha Oloko-Oba, and Serestina Viriri, "Pre-Trained Convolutional Neural Network for the Diagnosis of Tuberculosis." *International Symposium on Visual Computing, Springer, Cham*, pp. 558-569, 2020. *Crossref*, https://doi.org/10.1007/978-3-030-64559-5_44

[17] Yibin Wang, Haifeng Wang, and Zhaohua Peng, "Rice Diseases Detection and Classification using Attention based Neural Network and Bayesian Optimization," *Expert Systems with Applications*, vol. 178, p. 114770, 2021. *Crossref*, https://doi.org/10.1016/j.eswa.2021.114770

[18] K. Aravinth Raaj, B. Joel Sherwin, and S. Sabeetha Saraswathi, "Automated Detection of Abnormalities in Chest X-RayImages Using Convolutional Neural Networks," *International Journal of P2P Network Trends and Technology*, vol. 8, no. 2, pp. 18-24, 2018. *Crossref*, https://doi.org/10.14445/22492615/IJPTT-V8I2P404

[19] Maryam Rahimzad et al., "An Efficient Multi-Sensor Remote Sensing Image Clustering in Urban Areas via Boosted Convolutional Autoencoder (BCAE)," *Remote Sensing*, vol. 13, no. 13, p. 2501, 2021. *Crossref*, https://doi.org/10.3390/rs13132501

[20] [Online]. Available: https://www.kaggle.com/datasets/tawsifurrahman/tuberculosis-tb-chest-xray-dataset

[21] Moumen El-Melegy, Doaa Mohamed, and Tarek ElMelegy, "Automatic Detection of Tuberculosis Bacilli from Microscopic Sputum Smear Images Using Faster R-CNN, Transfer Learning and Augmentation," *Iberian Conference on Pattern Recognition and Image Analysis*, Springer, Cham, pp. 270-278, 2019. *Crossref*, https://doi.org/10.1007/978-3-030-31332-6_24

[22] Vinayakumar Ravi, Harini Narasimhan, and Tuan D. Pham, "EfficientNet-Based Convolutional Neural Networks for Tuberculosis Classification," *Advances in Artificial Intelligence, Computation, and Data Science, Springer, Cham*, pp. 227-244, 2021. *Crossref*, https://doi.org/10.1007/978-3-030-69951-2_9

[23] Haval T. Sadeeq et al., "A New Hybrid Method for Global Optimization Based on the Bird Mating Optimizer and the Differential Evolution," *2021 7th International Engineering Conference "Research & Innovation amid Global Pandemic (IEC), IEEE*, pp. 54-60, 2021. *Crossref*, https://doi.org/10.1109/IEC52205.2021.947614